Paper No. 7

THE RADIOMETRIC CALIBRATION & PERFORMANCE EVALUATION OF THE ASET FACILITY

J. D. Shoore, A. B. Dauger, R. P. Day and R. H. Meier,
McDonnell Douglas Astronautics Company,
Huntington Beach, California

ABSTRACT

The Advanced Sensor Evaluation and Test (ASET) Facility, which simulates physical and optical exoatmospheric environmental conditions, provides the capability for radiometric calibration of infrared sensors and astronomical telescopes. The techniques and procedures developed and used to calibrate the facility are discussed.

INTRODUCTION

The Advanced Sensor Evaluation and Test (ASET) Facility, Figure 1, was developed by the McDonnell Douglas Astronautics Company (MDAC), Huntington Beach, California, as part of the Space Simulation Laboratory. The facility offers the capability to measure selected performance parameters, providing a radiometric calibration for a variety of infrared sensors in a simulated space environment.

This calibration ensures known and accepted values for the collimator beam irradiance which is the irradiance at the entrance aperture of systems under test.

Any optical measurement system intended for operation in an exoatmospheric environment must receive a meaningful preflight calibration, which provides the basis both for an evaluation to verify the predicted performance capability of the optical system, and for the actual flight test data reduction and analysis.

Reliable techniques and procedures have been established to ensure a controlled measurement process which, under statistical analysis, provides the degree of precision and accuracy with which optical systems can be calibrated within the facility.

Because there are presently no national standards for the unique ASET Facility's operational environment, it is impossible to obtain an absolute measure of the irradiance. However, based upon experiments and calculations, values and limits have been established by MDAC. The precision of measurement is extremely good. When an absolute standard becomes available, the accuracy values presently given can be converted.

ASET FACILITY

The ASET Facility, whose schematic diagram is shown in Figure 2, consists of a stainless steel vacuum chamber with an inner cryoshroud housing an on-axis parabolic collimator, a radiant energy source assembly, a calibration monitor that subtends one portion of the collimated beam, and a pair of scanning mirrors that direct the radiant energy from another portion of the collimated beam into a sensor under test. All the optical elements consist of Kanigen coated aluminum, and their active surfaces are gold coated. Vacuum levels of 10^{-8} torr or better can be achieved with a multistage, contamination-free pumping system. A dense gas helium closed-cycle cooling system cools the cryoshroud and all other interior structures, components, and optical elements to a temperature of approximately 20 Kelvin, thereby producing an extremely low radiation background. Tests have shown that once stabilization at the cold operational temperature has occurred, there is no measurable degradation of the performance of the collimator assembly due to cooling.

Also associated with the facility is a clean room that can maintain the sensor under test in a class-100 clean environment, which is defined as one having no more than 100 particles of 0.5-μ diameter or larger per cubic foot of clean room volume. A special air shower and cover are used to protect the aperture of the sensor from contamination when the sensor is attached to the chamber interface.

COLLIMATOR

The collimator assembly, shown in Figure 2, consists of a 0.81-m parabola having a focal length of 3.02-m, and two 0.81-m by 1.06-m plano-folding mirrors. Its performance was found to be diffraction-limited for wavelengths longer than 8-μm. During development the spatial distribution of the collimated beam's flux density was assessed and the expected symmetry and uniformity were observed.

STANDARD SOURCE ASSEMBLY

The standard source assembly is shown in Figure 3. It consists of a blackbody-type source with a fixed frequency chopper and a set of stepped limiting apertures located in front of its cavity, with a second set of stepped variable apertures located at its exit aperture, and a special dual-surface reflector mounted inside the integrating cavity. The interior surface texture of the integrating cavity walls and one side of the dual-surface reflector was achieved by peening these surfaces with glass beeds of size 20-30 screen mesh. The selected aperture located at the blackbody cavity is imaged, either into the integrating cavity or onto the selected exit aperture of the integrating cavity, with unity magnification via a toric mirror and four folding plano-reflectors and the dual-surfaced reflector located

inside the integrating cavity. The exit aperture of the integrating cavity is located at the back focus of the source projector, which projects a 2.36-times-reduced image into the focal plane of the parabolic collimator.

The source assembly can be operated in three different modes, depending on the angular position of the dual-surfaced reflector inside the cavity. The specular surface reflection mode is used to directly image the blackbody cavity aperture onto the integrating cavity exit aperture, when high irradiance levels are required. In the diffuse reflection mode, the dual-surfaced reflector is rotated 180 degrees so that its peened surface is in position to diffusely deflect the radiant energy onto the integrating cavity's aperture. The lowest irradiance levels are achieved by rotating the dual-surfaced reflector into a position where it does not intercept the beam entering the cavity and where the diffuse side is facing the cavity's exit aperture. In this test mode, called the integrating cavity mode of operation, the beam first strikes a convex diffuse reflecting surface of a button-type insert mounted in the wall of the integrating cavity. The diffuse button reflects the radiant flux toward the front half of the integrating cavity, from which it is again diffusely reflected toward the diffuse surface of the dual-surfaced reflector. This surface now provides a uniform Lambertian radiant background for the integrating cavity exit aperture, and fills the field of view of the source projector.

In the specular mode of operation, the 8-mm blackbody is used exclusively; only the exit apertures of the integrating cavity are varied. In the two other modes, combinations of the two sets of variable apertures can be used to control the beam irradiance. Furthermore, in the integrating cavity mode, an attenuator plate can be rotated into the exit beam from the blackbody to obscure any desired portion from reaching the integrating cavity. The final result is that for any given blackbody temperature this source assembly can provide a range of irradiance values in the collimated beam that spans more than nine orders of magnitude. This is achieved without filters or impractical aperture sizes. The effective attenuation factor between the specular mode and the diffuse mode for a selected set of apertures is approximately 15.4, while the effective attenuation factor between the diffuse mode and the integrating cavity mode is approximately 600.

CALIBRATION MONITOR

The calibration monitor is mounted with the collimator assembly. It consists of a Cassegrainian telescope, referred to as the tester telescope, and a bolometer-type detector assembly. The tester telescope has a primary mirror 0.204 m in diameter, an F-number of 3.5, and an effective collection area of 211.6 cm^2. The optical performance of the tester telescope was measured and found to be diffraction-limited for all wavelengths greater than 3.5 μm. The tester telescope is mounted looking downward into the collimated beam of the ASET collimator, with its optical axis

parallel to the axis of the collimated beam. It intercepts a 0.2-m-diameter portion of the collimated beam adjacent to that portion of the beam which is used in testing systems. The bolometer assembly is mounted on a three-axis detector table, and its detector element is placed at the focal plane of the tester telescope.

BLACKBODY-TYPE SOURCE ASSEMBLY

The blackbody source assembly geometry is presented in Figure 4. The source assembly, which consists of the blackbody-type source, the baffling structure, stepped limiting apertures, and the fixed-frequency chopper, is mounted directly on the cooled three-axis source table. The dimensions of the source-limiting apertures vary in six discrete steps from 0.76 to 8.00 mm in diameter. The chopper is mounted on a shaft between the mounting plates and is driven through a nylon gear train by a fixed-frequency motor that mounts on the back side of the aperture plate in an enclosed radiation shield can. To ensure cooling of the apertures and the chopper blade, the blackbody is mounted on a separate mounting structure, with its heat sink achieved through a controlled heat leak directly to the actively cooled source table. The source table temperature is force-cooled to approximately 20-Kelvin. A 25-Kelvin maximum aperture temperature has been measured when the blackbody was operated at 300 Kelvin. The entire source assembly is covered, well baffled, and cooled to eliminate any unwanted energy.

The blackbody cavity is fabricated from ultra-pure aluminum (1100 series). At the time of the bolometer calibration the cavity was assumed to have a surface emissivity of 0.90, resulting in an effective calculated emissivity of 0.9977, determined according to the method of Gouffé. The cavity temperature at that time was monitored using a single copper: constantan thermocouple. Currently, the cavity temperature is monitored by three copper: constantan thermocouples embedded in its wall symmetrically around the apex of the cavity. The reference temperature used for the blackbody is liquid nitrogen.

At the time of the initial ASET Facility bolometer responsivity calibration, the blackbody radiant exitance (M) was determined by measurements of its temperature and calculation of its effective emissivity. The value used for the Stefan-Boltzmann constant was 5.6697×10^{-12} W-cm^{-2} K^{-4}, as per NAS-NRC Committee, 1963, NBS, U.S. Technical News Bulletin, No. 10, pp. 175-177.

BOLOMETER CALIBRATION

A high-quality gallium-doped germanium semiconductor bolometer supplied by Infrared Laboratories, Inc., was chosen as a working transfer standard. The philosophy for the ASET Facility calibration is based on the bolometer serving as the working standard, since the total irradiance in the collimated beam is established by bolometer measurements.

Normally, the blackbody and bolometer would be used together as a set of standards, one serving as a cross-check on the other, with the blackbody considered the primary working standard. However, it was decided to use the bolometer as the working transfer standard of total irradiance subsequent to its initial calibration with the blackbody. This decision was based on evidence that the bolometer performance characteristics are highly stable and repeatable over a long period of time, whereas the long-term repeatability of temperature settings of the blackbodies appears to be quite deficient.

The calibration of the bolometer consists of the determination of its blackbody responsivity; i.e., its responsivity with respect to the radiant energy emitted by a blackbody. The ASET blackbody was initially assumed to be the primary laboratory standard in the 100 to 400 Kelvin temperature region, providing standard values of irradiance (w/cm^2) over a range that satisfies the requirements for calibrating the bolometer.

The responsivity of the bolometer is determined from the output signal voltage ($V_{s,rms}$), with the bolometer viewing the blackbody cavity directly. The measured voltage is plotted as a function of the radiant power (ϕ_{BB}) incident upon it. The slope of the resulting calibration curve yields the blackbody responsivity of the bolometer, $R_{BB} = V_{s,rms}/\phi_{BB}$. Figure 5 presents a plot of the measured signal for a 25.5-Hz copper frequency as a function of the modulated radiant power incident on the bolometer. The bolometer responsivity was calculated at each point and was determined to be, $R_{BB} = 1.54 \pm 0.03 \times 10^5$ volts (rms)/watt (peak to peak). The resultant slope of the responsivity varied by ± 0.03 for a 1σ value. The bolometer has an effective sensitive area of one millimeter diameter and is operated at 2.03 Kelvin by carefully maintaining the vapor pressure in its helium dewar to within $\pm 10^{-3}$ torr.

The rss uncertainty of the radiant power for each of the data points shown in Figure 6 is represented by error bars. Because of the assumed ± 5-degree measurement uncertainty at all temperatures of the blackbody cavity, a larger uncertainty (longer bars) occurs for lower temperatures. A combination of different blackbody temperatures and various apertures and separation distances was used to obtain the range of radiant power, which accounts for the different-length error bars that occur along the graph.

The single-value bolometer responsivity calibration was accomplished for blackbody temperatures of 100, 200, and 300 Kelvin. As a result, a temperature of approximately 300 Kelvin can be chosen for determining the resulting rss uncertainty in the bolometer responsivity. At the time of the bolometer responsivity calibration, the rss uncertainty was determined to be ± 8.9 percent.

For the various source apertures, Figure 6 can be used to estimate the conversions to the rms value of the radiant power as referenced to the fundamental component of a square wave. The unit of radiant power, watts, refers to the total watts (peak-to-

peak) value of the square-wave-type modulated beam. In general, it is sufficient to multiply the watts peak-to-peak value by 0.45 to convert to watts rms of the fundamental. To convert to the rms value of the bolometer blackbody responsivity, the bolometer responsivity is multiplied by 2.22.

Recent noise measurements were made on the bolometer using the configuration shown in Figure 7. At a bolometer temperature of 2.03 Kelvin, a bias current of 0.5 microamperes (μA), and a QuanTech 304 TDL wave-analyzer noise equivalent bandwidth of 1 Hz, the mean bolometer noise was found to be 46 nV/$\sqrt{\text{Hz}}$ at 25.5 Hz.

Although the bolometer calibration was carried out at a single chopping frequency, 25.5 Hz, the measured frequency response of the bolometer is included in Figure 8. A typical noise spectrum is presented in Figure 9. This noise spectrum was recorded using a QuanTech 304 TDL spectrum analyzer operating with a 1-Hz bandwidth and a 25-db half-band response.

BEAM IRRADIANCE CALIBRATION THEORY

The bolometer is used as a working transfer standard during the irradiance calibration of the collimated beam. The blackbody responsivity of the bolometer is given by

$$R_{BB} = \frac{V_{SBN}}{\Phi_{BB} G_c} \left[\frac{\text{volts (rms)}}{\text{watts (p-p)}}\right] \tag{1}$$

where

V_{SBN} = the signal resulting from source and background irradiance and noise, referenced at the bolometer, in volts (rms)

G_c = electrical gain during responsivity calibration

Φ_{BB} = the radiant power, total watts peak-to-peak value of a square wave, and is given by

$$\Phi_{BB} = \frac{\varepsilon_{eff} \sigma T_{BB}^4 A_S A_D}{\pi S^2} \left[\text{watts (p-p)}\right] \tag{1A}$$

where

ε_{eff} = effective calculated emissivity of the blackbody cavity, per A. Gouffe, 0.9977

σ = Stefan-Boltzmann constant, 5.6697×10^{-12} W cm^{-2} K^{-4}

T_{BB} = blackbody cavity measured temperature in degrees Kelvin

A_S = area of source (i.e., area of blackbody variable aperture) in cm^2

A_D = area of bolometer, 7.85×10^{-3} cm^2

S = separation distance between source and bolometer during the bolometer calibration, cm

The calculated value of the bolometer responsivity, R_{BB}, when operated at 2.03 Kelvin and at a bias current of 0.5 μA, as given previously, is 1.54×10^5 volts (rms)/watts (p-p).

The radiant power incident on the bolometer when mounted at the focal plane of the tester telescope is given by

$$\Phi_{BB} = \frac{V_{SBN}}{R_{BB}} \left[\text{watts (p-p)}\right] \tag{2}$$

The total voltage out of the bolometer is a function of more than one variable, and is given by

$$V_{SBN} = \left[(V_S + V_B)^2 + V_N^2\right]^{1/2} \left[\text{volts (rms)}\right] \tag{3}$$

where

V_S = the signal out of the bolometer due to the modulated source in volts (rms)

V_B = the background radiation-contributed noise in volts (rms)

V_N = the bolometer noise in volts (rms)

Therefore, the total irradiance at the entrance aperture of the tester telescope is the same as the total irradiance in the collimator beam, and is given by

$$E_{SB} = \frac{\left(V_{SBN}^2 - V_N^2\right)^{1/2}}{G_E A_{TT} R_{BB}} \left[\frac{\text{watts (p-p)}}{\text{cm}^2}\right] \tag{4}$$

where

E_{SB} = the total irradiance from the modulated source and the DC background, in watts (p-p)/cm^2

V_{SBN} and V_N = same as before

G_E = the electrical gain during the irradiance calibration

A_{TT} = the effective area of the entrance aperture of the tester telescope, 211.6 cm^2

R_{BB} = the responsivity of the bolometer, 1.54×10^5 v (rms)/w(p-p), with a ± 8.9 percent rss uncertainty

RESULTS

The total source irradiance, E_{SB}, in the ASET collimator beam is presented for each calibration temperature as a function of the normalized effective aperture diameters and for each mode as defined by the position of the beam deviating mirror mounted within the integrating cavity. The normalized effective aperture

diameters (NEAD) is defined as

$$\text{NEAD} = \left[\left(\frac{\text{source aperture diameter}}{8.00}\right)\left(\frac{\text{IC aperture diameter}}{5.88}\right)\right]^2 \quad (5)$$

where each aperture is normalized to the largest aperture in its set.

The average blackbody temperatures at which the beam irradiance calibration was performed were 400.2, 300.1, and 200.6 Kelvin. As explained previously, the three modes defined by the position of the beam-deviating mirror are specular, diffuse, and integrating cavity. The numbers associated with each measured point represent the aperture combination identification. Those points which are solid indicators without the associated rss error bar could not be measured with the bolometer, i.e., $E_{SB} \leq$ NEI (noise equivalent irradiance) of the bolometer. They are included, however, since the area relationships are maintained between apertures, and hence the associated irradiance value can be extrapolated.

The results are presented in Figures 10, 11, and 12. Also, Figure 13 presents the normalized effective diameter code that defines the aperture combinations used to achieve the irradiance levels for the various modes of operation. The measured data points are presented with the rss error bar limits resulting from the geometric and bolometer responsivity uncertainties. Data analysis indicates that the bolometer responsivity appears to be independent of the blackbody temperature. Therefore, the temperature error of the blackbody during the irradiance calibrations is not of prime importance in the error budget for the beam irradiance. As a result, the rss uncertainty in the responsivity of the bolometer calibration is increased only by the additional measurement errors encountered in determining the total beam irradiance. Thus, the rss uncertainty in the total beam irradiance is given as ± 9.22 percent.

A comparison between the graphs generated for the three different blackbody temperatures shows excellent agreement with the Stephan-Boltzmann law, which may be verified by comparing the ratio of the total irradiances to the ratio of the temperatures raised to the fourth power. For the beam-deviating mirror in the diffuse mode, the ratios are performed and presented. As may be seen, the comparison of measured versus ratio differences are less than 1 percent.

$$\left(\frac{400.2}{300.1}\right)^4 = 3.16; \quad \frac{E_{BB\ 400.2}}{E_{SB\ 300.1}} = 3.14; \quad \text{percent difference} = 0.63$$

$$\left(\frac{300.1}{200.6}\right)^4 = 5.01; \quad \frac{E_{SB\ 300.1}}{E_{SB\ 200.6}} = 5.00; \quad \text{percent difference} = 0.20$$

$$\left(\frac{400.2}{200.6}\right)^4 = 15.84; \quad \frac{E_{SB\ 400.2}}{E_{SB\ 200.6}} = 15.70; \quad \text{percent difference} = 0.88$$

Additionally, checks were made to determine the variation between the irradiance levels as established by the beam-deviating mirror positions. The variations were found to remain constant as a function of the temperature and geometric changes. This tends to indicate a lack of dependence upon the wavelength as a function of temperature and variable geometries.

A regression analysis utilizing a two-variable power regression of the form

$$y = A_o x^{A_1} \tag{6}$$

has been performed to allow for rapid calculation of irradiance levels for sensor calibrations. The relationship is linear on a log-log plot, and the slope of the line is very close to unity. As such, the data are described extremely well. All the measured data were entered to determine the coefficients of the power curve. Once the coefficients were determined, the best-fit line for the data was plotted. As can be seen in Figures 10 through 12, the best-fit calculated curve describes the measured data. The correlation coefficient approaches unity for each case, providing an estimate of the overall precision of the measurements.

REPEATABILITY OF DATA

During the pumpdowns after the calibration run, comparison data were taken with the bolometer to see if there were any variations that could be attributed to test buildup or lapsed time between measurements. Presented in Table 1 is a comparison of the raw voltage data taken on 17 May 1972, during the original calibration, and verification data taken on 30 May and 10 October 1972. As shown, the worst-case percent difference for each beam-deviating mirror position is 3 percent for the low-energy integrating cavity mode measurements.

ERROR ANALYSIS

The total irradiance in the beam of the collimator has been examined in sufficient detail to provide for an rss error uncertainty determination. An estimate of the accuracy of the beam irradiance can be obtained by determining the absolute fractional error in E_{SB}, Equation (4), which is given by the summation of the differential dE_{SB} divided by the true value of E_{SB}. This can be written in equation form and is given by

$$\frac{dE_{SB}}{E_{SB}} = \frac{1}{E_{SB}} \sum_{X_i} \frac{\partial E_{SB}}{\partial S_i} dX_i, \tag{7}$$

where X_i indicates the set of independent variables of Equation (4). Expanding Equation (4) as a function of all terms in the responsivity equation gives

$$E_{SB} = \frac{\left(V_{SBN}^2 - V_N^2\right)^{1/2} G_C \varepsilon_{eff} \sigma T_{BB}^4 A_S A_D}{\pi G_E A_{TT} S^2 V_1} \left[\frac{\text{watts (p-p)}}{\text{cm}^2}\right] \quad (8)$$

where all terms are as defined previously except for

V_1 = the bolometer voltage output during the bolometer calibration, in volts (rms)

Before proceeding with the error analysis, some mention should be made of the case where the background-contributed noise voltage exceeds the bolometer noise voltage, i.e., $V_B > V_N$. Normal operating conditions of the ASET Facility are such that $V_B << V_N$. However, during unusual measurement conditions there have been occasions when measurable background irradiance was observed. It is for this reason that subscripts denoting background are included in the expression for the total irradiance. Under such adverse conditions, where $V_B > V_N$, it should be recognized that a meaningful error analysis cannot be carried out. The effect of high background is easily observed, and must be corrected before calibration measurement is performed. In typical operation the inherent low background in the ASET Facility does not influence the bolometer calibration. If a very low background is found to be present, the following two criteria for acceptable data in the presence of the background noise can be considered. First, only those data points are considered for which the signal voltage $V_S \geq 9V_B$ (or in terms of measurable quantities, one has $(V_S + V_B) \geq 10V_B$. Secondly, the decision to accept or reject a particular data point must be influenced by the technical judgement of the scientist conducting the measurements. Based upon these criteria, variations of E_{SB} with V_B in the following analysis may be ignored.

Now, performing the substitution of Equation (8) into Equation (7) and evaluating the partial derivative yields

$$\left[\frac{dE_{SB}}{E_{SB}}\right] = \left[\frac{V_{SBN}\, dV_{SBN} - V_N dV_N}{V_{SBN}^2 - V_N^2}\right] + \left[\frac{d\varepsilon_{eff}}{\varepsilon_{eff}}\right] + \left[\frac{d\sigma}{\sigma}\right] + \left[\frac{4dT_{BB}}{T_{BB}}\right] + \left[\frac{dA_S}{A_S}\right] + \left[\frac{dG_C}{G_C}\right] + \left[\frac{dA_D}{A_D}\right] - \left[\frac{dG_E}{G_E}\right] - \left[\frac{dA_{TT}}{A_{TT}}\right] - \left[\frac{2dS}{S}\right] - \left[\frac{dV_1}{V_1}\right] \quad (9)$$

In order to simplify computations, an approximation is considered for the first term of Equation (9). It is desirable to eliminate the relative error in the noise voltage, dV_N/V_N, because measuring

dV_N/V_N with high precision is difficult. Therefore, in general, only those data points for which $V_{SBN}/V_N \geq 2$ are deemed acceptable. Using this assumption, the first term in Equation (9) can be approximated as

$$\frac{V_{SBN}\, dV_{SBN} - V_N\, dV_N}{V_{SBN}^2 - V_N^2} = \left[\frac{1}{1 - \left(\frac{V_N}{V_{SBN}}\right)^2}\right]\left[\frac{dV_{SBN}}{V_{SBN}}\right] - \left[\frac{1}{\frac{V_{SBN}^2}{V_N} - 1}\right] \quad (10)$$

$$\left[\frac{dV_N}{V_N}\right] \approx \frac{dV_{SBN}}{V_{SBN}} \text{ within 1 percent.}$$

Equation (9) can be rewritten as simplified by Equation (10) and then converted in terms of the rss uncertainty in the total irradiance by taking the square root of the sum of the squares of each term. Thus, the rss uncertainty in the total irradiance is given by

$$\left[\frac{dE_{SB}}{E_{SB}}\right]_{rss} = \pm \left[\left(\frac{dV_{SBN}}{V_{SBN}}\right)^2 + \left(\frac{d\varepsilon_{eff}}{\varepsilon_{eff}}\right)^2 + \left(\frac{d\sigma}{\sigma}\right)^2 + \left(\frac{4dT_{BB}}{T_{BB}}\right)^2 + \left(\frac{dA_S}{A_S}\right)^2 + \left(\frac{dA_D}{A_D}\right)^2 + \left(\frac{dG_C}{G_C}\right)^2 + \left(\frac{dA_{TT}}{A_{TT}}\right)^2 + \left(\frac{2dS}{S}\right)^2 + \left(\frac{dV_1}{V_1}\right)^2 + \left(\frac{dG_E}{G_E}\right)^2\right]^{1/2} \quad (11)$$

A summary of the assumed and measured uncertainties in Equation (11) is given in Table 2. As can be seen, the dominant error lies in the assumed ± 5-degree uncertainty in the blackbody temperature measurement at the time of the responsivity calibration. Since the variation in the responsivity was only ± 0.03 for a 1σ value for the various temperatures used in the responsivity calibration, the highest calibration temperature is used in determining the rss uncertainty, i.e., 300 Kelvin. The beam irradiance measurement is dependent upon the bolometer calibration and hence, the blackbody temperature is not found in the beam irradiance undertainties summary. Solving Equation (11) using the values of Table 2 gives an rss uncertainty in the total beam irradiance of ± 9.22 percent.

522-137 O - 73 - 7

SOURCE MONOCHROMATOR

In addition to the total irradiance calibration capability, the ASET Facility has another source assembly capable of producing a scanable monochromatic beam, thus providing the capability for spectral response calibrations. The spectral range covered is from 2.5 to 26 micrometers. The monochromator source assembly replaces the standard source assembly on the source table, with its radiant output projected with the same F-number into the collimator through a single fixed exit aperture. It is an all-reflective grating instrument whose use has important advantages over the use of narrow-band filters to provide the necessary spectral energy distribution. A schematic diagram of the monochromator source is shown in Figure 14. It produces a nearly monochromatic beam that is focused onto the exit aperture and is then collimated by the ASET collimator, thus simulating a monochromatic point source at infinite distance.

The monochromator utilizes a filter wheel containing up to six multiple-layer interference-type longwave-pass filters. They are used to block radiation of shorter than selected wavelength values in order to prevent second-order and higher-order wavelength radiation output from the monochromator. In addition, one position can hold a polystyrene filter to serve as a wavelength calibrator.

Three gratings are available with rulings of 20, 40, and 80 lines per millimeter, corresponding to a line spacing of 50, 25, and 12.5 micrometers, and blaze wavelengths of 4.3, 8.6, and 17.2 micrometers respectively.

MONOCHROMATOR CALIBRATION

The main monochromator parameter to be calibrated is its output wavelength as a function of grating angle. This parameter is important since it remains constant from run to run, whereas the resulting beam irradiance depends on the blackbody-type source temperature. The variability of the irradiance is effectively taken into account by continuously measuring the beam irradiance with the calibration monitor, whose response is spectrally flat. Although three gratings are available, only two were calibrated, the 80 lines per mm and the 20 lines per mm. These two gratings cover the range from 2.5 to 26 micrometers in the first order, with a slight dip in the mid-range.

The expected wavelength values in the first order are given by

$$\lambda = 2d \sin\phi \cos\delta$$

with ϕ being the grating angle, δ the angle of incidence at the specular (zero order) position ($\phi = 0$), and d the line spacing or grating constant. For the 20 lines/mm grating at room temperature d = 50 μm, and for the 80 lines/mm grating d = 12.5 μm. The value of d is reduced at 20°K by 0.4 percent due to the contraction of the aluminum grating material. The value of cos δ is

0.86, based on the geometry of the instrument. It will not change with temperature, since the whole instrument is made of aluminum and should shrink uniformly, keeping angular relationships constant.

At room temperature the calculated wavelength values for each grating are

$$\lambda = 86.0 \sin\phi \quad (20 \text{ lines/mm})$$
$$\lambda = 21.5 \sin\phi \quad (80 \text{ lines/mm})$$

and at 20°K, the calculated wavelength values for each grating are

$$\lambda = 85.65 \sin\phi \quad (20 \text{ lines/mm})$$
$$\lambda = 21.42 \sin\phi \quad (80 \text{ lines/mm})$$

The grating was directly connected to a rotary resolver, i.e., an angular position transmitter, whose output signals were converted to digital information and input directly to a digital computer, a PDP-15, which calculated the wavelength according to the preceding formulas and displayed it on a terminal at the ASET console in near real time. In addition, the bolometer signal output amplitude from the ASET lock-in amplifier (PAR HR-8) was input to the computer for display along with the wavelength. An X-Y recorder was also set up to plot the resolver analog signal along the X-axis and the lock-in amplifier signal along the Y-axis. This data-taking arrangement during an actual wavelength scan produced an analog plot of sensor signal versus wavelength simultaneous with a digital table of sensor signals as a function of wavelength as provided by the computer.

A typical room temperature monochromator response using the polystyrene filter is given in Figure 15. The corresponding response at 20 Kelvin is given in Figure 16. The wavelengths calculated from the formulas shown were compared with the polystyrene band center wavelengths. The discrepancies were within the monochromator resolution. Similar response curves using the interference type filters showed the expected 1 to 3 percent downward shifts in their characteristic wavelengths as the temperature was lowered to 20 Kelvin.

The measured results are presented in Table 3 for the 80 lines/mm grating and in Table 4 for the 20 lines/mm grating. The grating wavelengths are calculated using the previous formulas.

The monochromatic beam irradiance was measured using the ASET bolometer. The result was a set of typical system response curves of the monochromator and ASET Facility, which are presented in Figure 17. The curves were obtained with a 900 Kelvin source during two test cycles; one with the 80 lines per millimeter grating and the other with the 20 lines per millimeter grating.

The relative spectral response of a Si:As detector was obtained during tests within the facility, and is shown in Figure 18.

MONOCHROMATOR ERROR ANALYSIS

The major error in the monochromator wavelength calibration is due to the monochromator dispersion, which is 0.05 μm/mm for the 80 lines/mm grating and 0.22 μm/mm for the 20 lines/mm grating. During the operational tests in ASET, a 1.1 mm diameter aperture was used as the exit slit, so that the wavelength spread in the ASET beam was 0.055 μm and 0.25 μm respectively for each grating. During the ambient calibration runs using the thermocouple detector, the wavelength spread was defined by the 0.5 mm thermocouple width that was being used. The resulting expected wavelength uncertainty was therefore estimated to be 0.028 μm for the 80 lines/mm grating and 0.11 μm for the 20 lines/mm grating.

Other wavelength errors included offset in the analog-to-digital converter and graph reading error. The total wavelength errors due to these and other sources is about ± 0.02 μm for the 80 lines/mm grating and ± 0.08 μm for the 20 lines/mm grating. The total error in the monochromator wavelength calibration is therefore about ± 0.04 μm for the 80 lines/mm grating and ± 0.14 μm for the 20 lines/mm grating. It is seen in Tables 3 and 4 that the differences between measured and calculated wavelength values for each grating at any point are less than the calibration measurement errors. Therefore, the approach taken is considered sufficiently accurate to define the monochromator wavelength calibration.

REFERENCES

Day, R. P., Meier, R. H., Shoore, J. D., and Thompson, C. J. C.; Status Report on MDAC's Advanced Subsystem Evaluation and Test (ASET) Facility; MDAC-WD 1525, Nov 1970 (S).

Meier, R. H., Day, R. P., Shoore, J. D., and Thompson, C. J. C.; An Advanced Test and Evaluation Facility for Space Optical Systems; MDAC-WD 1573, Apr 1971 (C).

Shoore, J. D. and Day, R. P.; Calibration of the ASET Facility Bolometer; MDAC-G2484, Sept 1971.

Dauger, A. B., Meier, R. H., and Shoore, J. D.; Irradiance and Spectral Calibration of the MDAC ASET Facility; MDAC-WD 2081, Jan 1973.

Gauffé, A.; Corrections d'ouverture des corps-noirs artificiels compte tenu des diffusions multiples internes, Revue D'optique, 24, No. 1-3, Paris, France, 1945.

Holscher, H. H.; Simplified Statistical Analysis, Cahners Publishing Co., Inc., Bostin, Mass, 1971.

ACKNOWLEDGMENT

The authors particularly wish to acknowledge the team effort and contributions made by Messrs. J. R. Averett, F. A. Eckhardt, R. A. Edgell, W. A. Fraser, S. Griffith, R. M. Hartman, J. T. Morrow, R. E. King, B. C. Moore, E. J. Pisa, H. Popick, R. W. Powell, R. E. Schatzmann, I. Richman, E. H. Schwiebert, J. P. Theriault, and C. J. C. Thompson for their efforts in solving several unusual engineering problems in optics, mechanics, cryogenics, and vacuum technology which has greatly contributed to the successful completion of this unique facility. Also, we wish to express our appreciation for many fruitful discussions with Drs. R. H. McFee and S. Zwerdling. The work described here was conducted by the McDonnell Douglas Astronautics Company as part of the Company-sponsored research and development program.

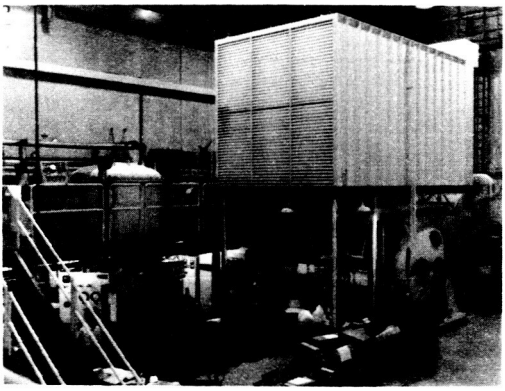

Figure 1. View of Test Facility

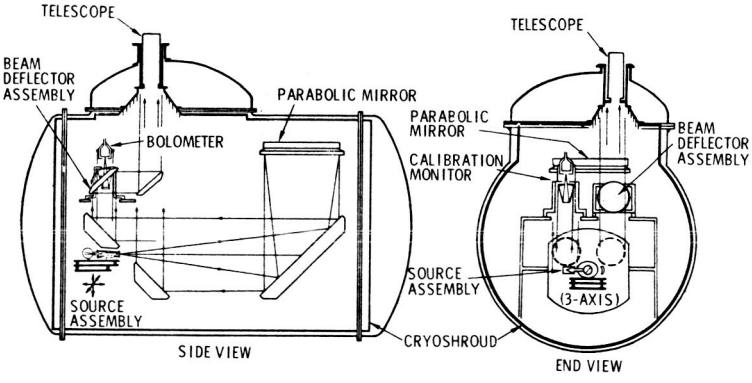

Figure 2. Schematic of ASET Facility

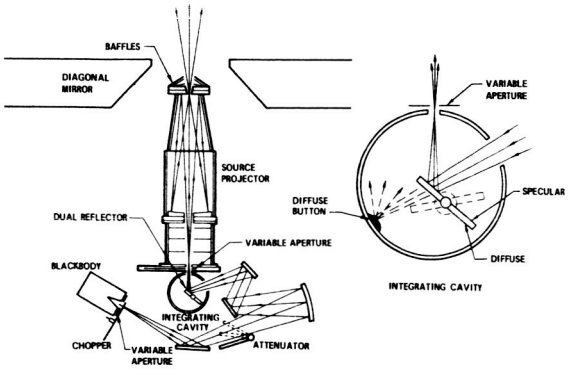

Figure 3. Standard Source Assembly

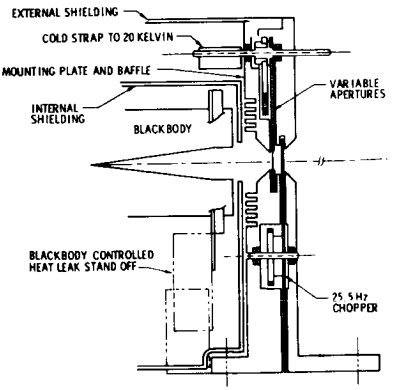

Figure 4. Blackbody Source Assembly

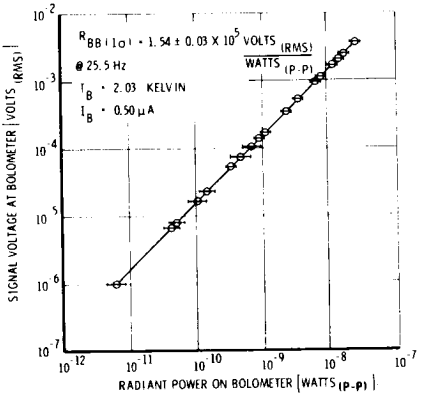

Figure 5. Bolometer Responsivity

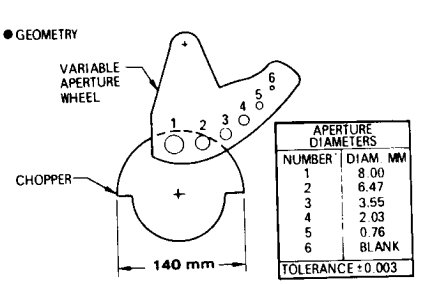

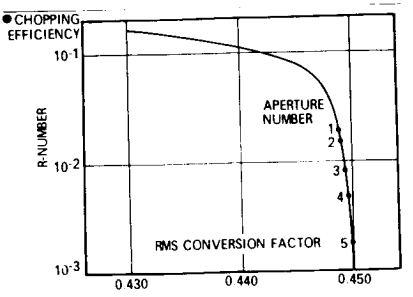

Figure 6. Source Chopper Temporal Variations

- MEASUREMENT CONFIGURATION & ANALYSIS

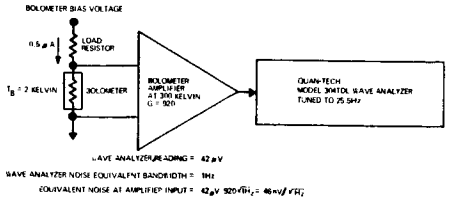

- NOISE CONTRIBUTORS
  1. JOHNSON NOISE OF BOLOMETER ($\overline{e}_b$ = 5nV/$\sqrt{Hz}$) AT 2 KELVIN
  2. JOHNSON NOISE OF LOAD RESISTOR ($\overline{e}_{RL}$ = 22nV/$\sqrt{Hz}$) AT 2 KELVIN
  3. EXCESS CURRENT NOISE OF BOLOMETER ($\overline{i}_b$ = 3 X 10^{-14} amp/$\sqrt{Hz}$) AT 2 KELVIN
  4. AMPLIFIER CURRENT NOISE ($\overline{i}_a$ = 1 X 10^{-14} amp/$\sqrt{Hz}$) AT 300 KELVIN
  5. AMPLIFIER VOLTAGE NOISE ($\overline{e}_a$ = 8nV/$\sqrt{Hz}$) AT 300 KELVIN

Figure 7. Noise Measurement & Analysis

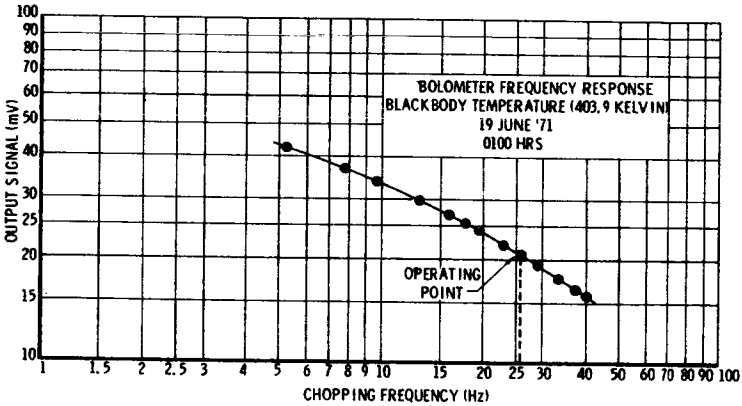

Figure 8. Bolometer Frequency Response

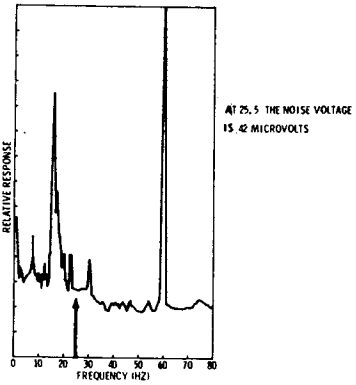

Figure 9. Bolometer Noise Spectrum

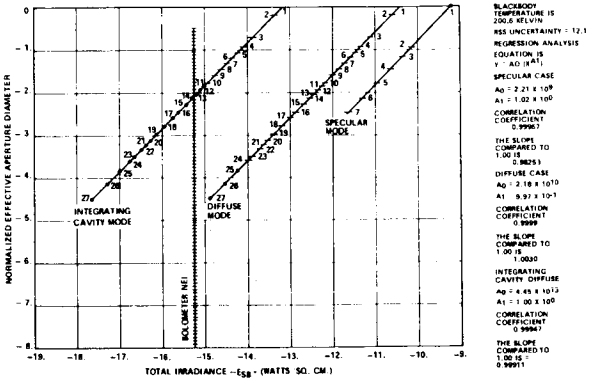

Figure 10. ASET Collimated Beam Total Irradiance, 200 Kelvin

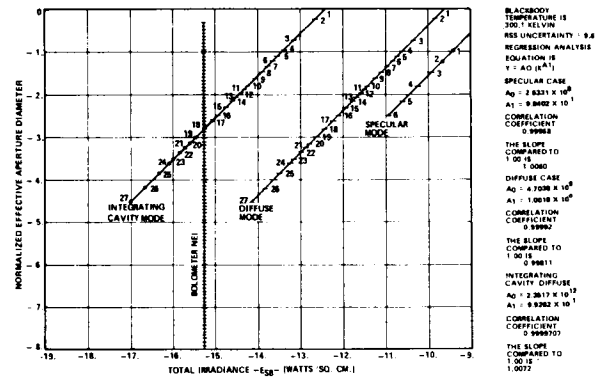

Figure 11. ASET Collimated Beam Total Irradiance, 300 Kelvin

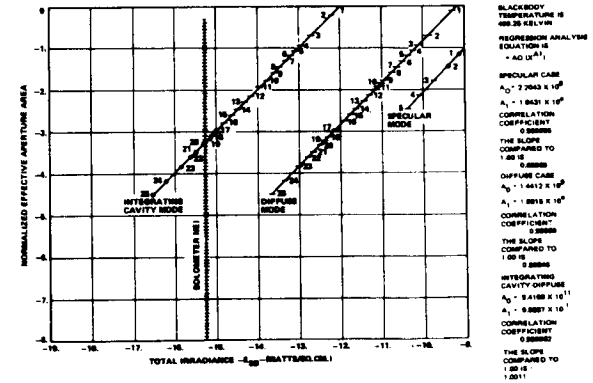

Figure 12. ASET Collimated Beam Total Irradiance , 400 Kelvin

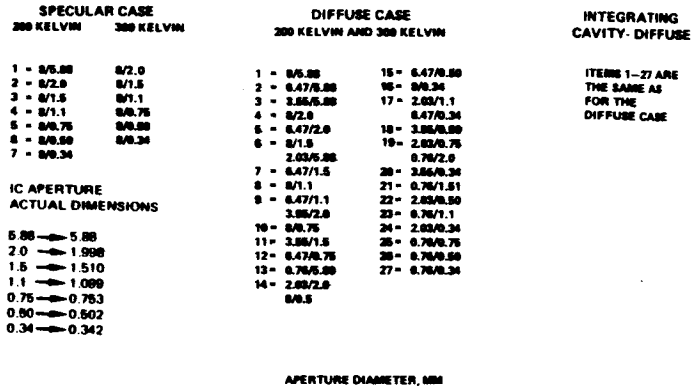

Figure 13. Effective Aperture Code

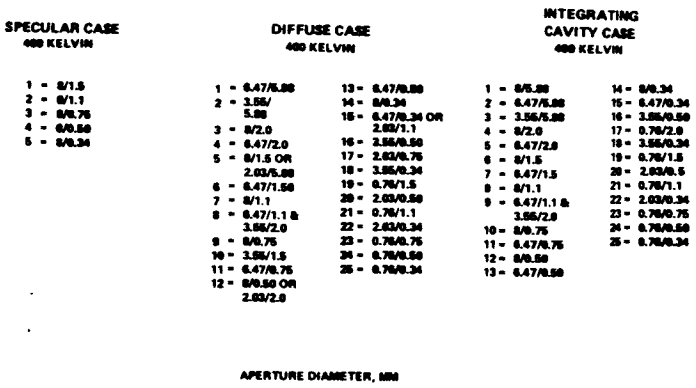

Figure 13A. Effective Aperture Code, T = 400 Kelvin

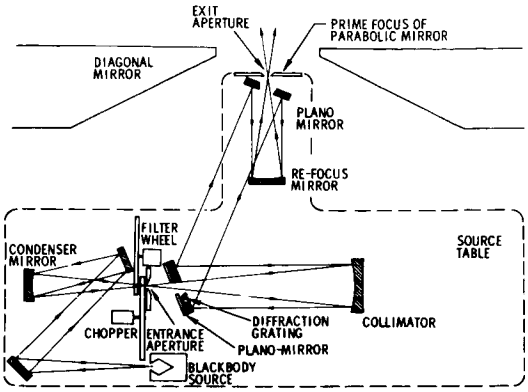

Figure 14. Monochromator Source

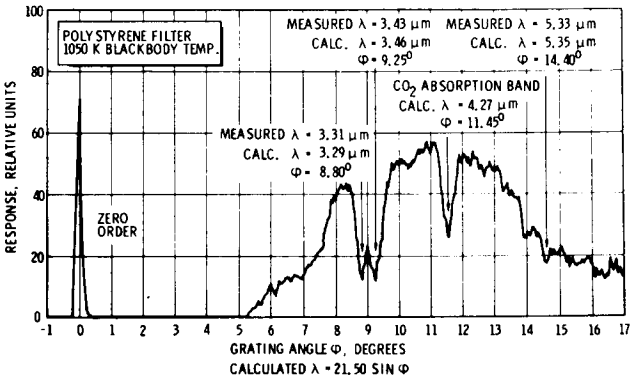

Figure 15. 80 Lines/MM Grating Calibration, Warm

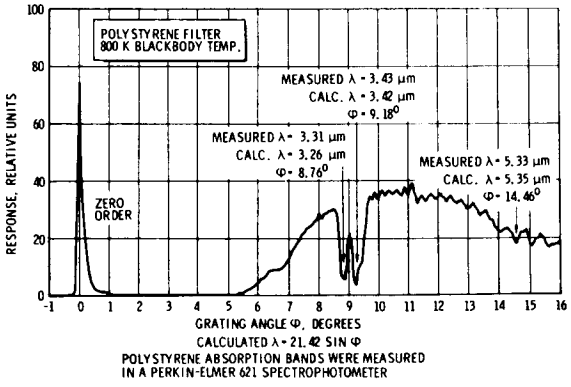

POLY STYRENE ABSORPTION BANDS WERE MEASURED IN A PERKIN-ELMER 621 SPECTROPHOTOMETER

Figure 16. 80 Lines/MM Grating Calibration, Cold

80 LINE/MM GRATING	
FILTER 1	2.2 – 4.0 μM
FILTER 2	3.9 – 6.6 μM
FILTER 3	5.9 – 8.0 μM
20 LINE/MM GRATING	
FILTER 4	8.0 – 12.3 μM
FILTER 5	10.2 – 19.4 μM
FILTER 6	18.2 – 26.0 μM

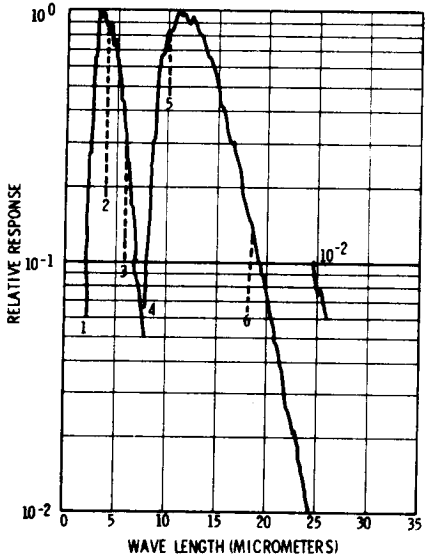

Figure 17. System Response of Monochromator

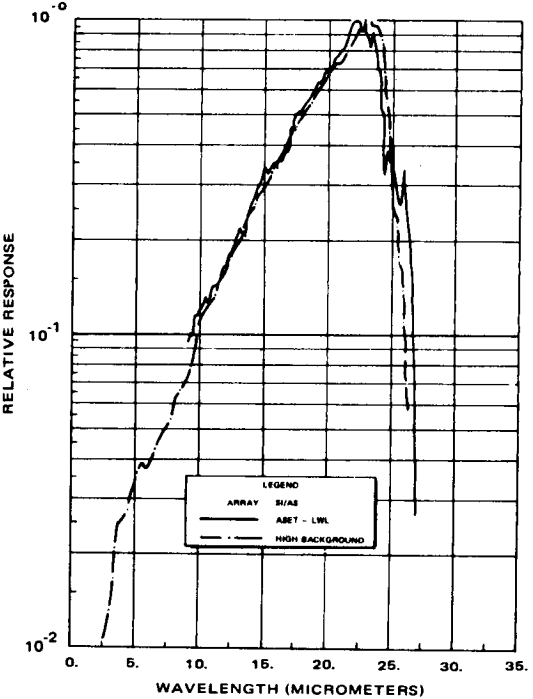

Figure 18. Spectral Response

APERTURE COMBINATIONS (mm)	SPECULAR MODE (VOLTS)			DIFFUSE MODE (VOLTS)		INTEGRATING CAVITY MODE (MILLIVOLTS)	
	17 MAY	30 MAY	10 OCT	17 MAY	30 MAY	17 MAY	30 MAY
8/5.88				6.55	6.65	10.4	10.3
8/2				0.760	0.765	1.21	1.2
8/1.5				0.447	0.440	0.680	0.69
8/1.1				0.243	0.245	0.355	0.36
8/0.75	1.64	1.65	1.65	0.106	0.105	0.165	0.160
8/0.50	0.7	0.7	0.7	0.047	0.047	0.075	0.075
8/0.34	0.335	0.335	--	0.022	0.022	0.034	0.035
PERCENT DIFFERENCE (WORST CASE)	≈ 0.6 PERCENT			≈ 0.9 PERCENT		≈ 3 PERCENT	

Table 1. Comparison of Voltage Data Taken On May 1972 With Data Taken On 30 May 1972 and 10 October 1972

UNCERTAINTIES IN BOLOMETER RESPONSIVITY CALIBRATION		UNCERTAINTIES IN BEAM IRRADIANCE CALIBRATION	
>1 PERCENT	<1 PERCENT	>1 PERCENT	<1 PERCENT
$4dT_{BB}T_{BB}$ at 300°K = 6.7×10^{-2} and dT = 5-degrees	dA_S/A_S = 4.44×10^{-5}	dV_{SBN}/V_{SBN} = 2.0×10^{-2}	dA_{TT}/A_{TT} = 1.0×10^{-3}
$d\varepsilon_{eff}/\varepsilon_{eff}$ = 5.0×10^{-2}	dA_D/A_D = 1.0×10^{-3}	dG_E/G_E = 1.0×10^{-2}	
dG_C/G_C = 1.0×10^{-2}	$2d\delta/\delta$ = 3×10^{-3}		
dV_1/V_1 = 3.0×10^{-2}	$d\omega/\sigma$ = 5.1×10^{-4}		

Table 2. Summary of RSS Uncertainties

MEASURED WAVELENGTH	ROOM TEMPERATURE, IN AIR		20 K, IN VACUUM	
	GRATING ANGLE	WAVELENGTH	GRATING ANGLE	WAVELENGTH
POLYSTYRENE 3.31 μm	8.80°	3.29 μm	8.76°	3.26 μm
POLYSTYRENE 3.43 μm	9.25°	3.46 μm	9.18°	3.42 μm
POLYSTYRENE 5.33 μm	4.40°	5.35 μm	14.46°	5.35 μm
CO_2 ABSORPTION BAND 4.27 μm	11.45°	4.27 μm	NONE	

Table 3. 80 Lines/mm Grating Calibration

MEASURED WAVELENGTH	ROOM TEMPERATURE, IN AIR		20 K, IN VACUUM	
	GRATING ANGLE	WAVELENGTH	GRATING ANGLE	WAVELENGTH
POLYSTYRENE 13.33 μm	8.85°	13.32 μm	8.95°	13.33 μm
POLYSTYRENE 14.40 μm	9.60°	14.40 μm	9.60°	14.37 μm

Table 4. 20 Lines/mm Grating Calibration